Study of the Electronic Structure, Metal–Metal Bonding, and Ground-State Exchange Coupling in Face-Shared $Mo_2X_9^{3-}$ (X = Cl, Br, I) Dimers Using the Broken-Symmetry Xα–SW Method

Gregory A. Medley and Robert Stranger*

Department of Chemistry, The University of Queensland, Brisbane, QLD 4072, Australia

Received March 18, 1994®

The results of spin-restricted SCF–Xα–SW and spin-unrestricted broken-symmetry SCF–Xα–SW calculations on the face-shared dimer complexes $A_3Mo_2Cl_9$ (A = K, Rb, Cs, Me_4N), $A_3Mo_2Br_9$ (A = Cs, Me_4N), and $Cs_3Mo_2I_9$ are reported and used to discuss the electronic structure, metal–metal bonding, and magneto–structural correlations in these systems. The spin-restricted SCF–Xα–SW ground-state calculations on $Cs_3Mo_2X_9$ (X = Cl, Br, I) show that the metal–metal σ and π bonding interactions are significantly reduced for the bromide and especially for the iodide complex relative to $Mo_2Cl_9^{3-}$, consistent with the increased metal–metal bond distances observed for both these complexes. The ground-state exchange interaction is shown to be almost entirely the result of direct overlap of magnetic orbitals with negligible contribution from superexchange effects. The Xα–SW calculations for the broken-symmetry ground state reveal that the magnetic orbitals involved in the metal–metal π interaction are almost completely localized on the metal ions. The magnetic orbitals involved in the metal–metal σ interaction, on the other hand, are partially delocalized between the two metals but still contribute significantly to the ground-state exchange interaction in agreement with earlier spectroscopic and theoretical studies. The calculated exchange coupling constants J_{ab} for the complexes $Cs_3Mo_2X_9$ (X = Cl, Br, I) support this conclusion and indicate that the effective maximum spin in the ground-state exchange levels lies between 2 and 3. A significant antiferromagnetic contribution arises from ligand → metal spin-polarization effects which accounts for the unusually large $-J_{ab}$ value found for the iodide complex. The magneto–structural correlations observed for the chloride and bromide complexes have been successfully modeled by initially using Mo atomic sphere radii which reproduced the experimental J_{ab} values for $Cs_3Mo_2Cl_9$ and $Cs_3Mo_2Br_9$ and then adjusting the Mo sphere radii for the remaining complexes in proportion to their metal–metal bond distances relative to the Cs salts.

Introduction

Much effort has been focused in the last 20 years or so on describing the electronic structure of dimeric complexes containing multiple metal–metal bonds.[1] In particular, quadruple metal–metal-bonded complexes have received the greatest attention, both bridged and unsupported varieties, and to a lesser extent metal–metal triple-bonded species. In more recent years, the use of density functional methods[2-6] and the relative ease of incorporation of relativistic effects have played an important role in electronic structure calculations and have led to significant advances in our understanding of metal–metal bonding interactions. In addition, the broken-symmetry Xα–SW approach[7,8] (also known as the Xα–valence bond method) has been quite successful in probing the magnetic interactions in relatively weakly coupled dimers as well as the calculation of ground-state exchange coupling constants in such complexes.[9-13]

In contrast with multiple metal–metal-bonded complexes and weakly coupled dimers, very few electronic structure calculations have appeared on dimeric complexes involving intermediate metal–metal bonding, though this may well be attributed to the limited number of systems exhibiting such interactions. The face-shared bioctahedral complexes $Mo_2X_9^{3-}$ (X = Cl, Br, I) are a classic dimer series intermediate between the weakly coupled $Cr_2X_9^{3-}$ and strongly metal–metal-bonded $W_2X_9^{3-}$ dimer systems. The intermediate nature of the metal–metal bonding interactions in the $Mo_2X_9^{3-}$ complexes is highlighted by the dramatic sensitivity of the metal–metal distance and ground-state exchange coupling constant J_{ab} to the size of the univalent counterion, A, in the complex salts $A_3Mo_2X_9$.[14,15] The close-packing arrangement causes an expansion of the $Mo_2X_9^{3-}$ dimeric unit along the metal–metal axis when the size of the univalent cation A is increased.

Detailed spectroscopic studies[16-19] on the $Cs_3Mo_2Cl_9$ and $Cs_3Mo_2Br_9$ complexes have shown that although the metal–metal σ interaction is quite strong, resulting in a partial factoring-out of two electrons into a metal–metal σ bond, the metal–metal π interaction is comparatively weak and largely responsible for the exchange splitting observed in the excited-state pair multiplets. However, although the excited-state multiplet splittings are predominantly the result of the metal–metal π interaction, theoretical studies[20] on the d^3d^3 exchange-coupled pair system have shown that, even for moderate to strong metal–metal σ bonding, the two electrons involved in the metal–metal σ interaction may still contribute significantly to the ground-state exchange coupling but in this case the exchange splitting of the ground-state spin levels will not be correctly described by the Heisenberg spin Hamiltonian $\mathcal{H}_{ex} = -2J_{ab}S_a \cdot S_b$.

* Author to whom correspondence should be addressed.

® Abstract published in *Advance ACS Abstracts*, July 1, 1994.

(1) Cotton, F. A.; Walton, R. A. *Multiple Bonds between Metal Atoms*, 2nd ed.; Clarendon: Oxford, 1993.
(2) Slater, J. C. *The Self-Consistent Field for Molecules and Solids: Quantum Theory of Molecules and Solids*; McGraw-Hill: New York, 1974; Vol 4.
(3) Johnson, K. H. *Adv. Quantum Chem.* **1973**, *7*, 143.
(4) Johnson, K. H. *Annu. Rev. Phys. Chem.* **1975**, *26*, 39.
(5) Case, D. A. *Annu. Rev. Phys. Chem.* **1982**, *33*, 151.
(6) Ziegler, T. *Pure Appl. Chem.* **1991**, *63*, 873.
(7) Noodleman, L.; Norman, J. G., Jr. *J. Chem. Phys.* **1979**, *70*, 4903.
(8) Noodleman, L. *J. Chem. Phys.* **1981**, *74*, 5737.
(9) Bencini, A.; Gatteschi, D. *J. Am. Chem. Soc.* **1986**, *108*, 5763.
(10) Albonico, C.; Bencini, A. *Inorg. Chem.* **1988**, *27*, 1934.
(11) Bencini, A. *J. Chim. Phys.* **1989**, *86*, 763.
(12) Ross, P. K.; Solomon, E. I. *J. Am. Chem. Soc.* **1991**, *113*, 3246.
(13) Noodleman, L.; Baerends, E. J. *J. Am. Chem. Soc.* **1984**, *106*, 2316.
(14) Stranger, R.; Grey, I. E.; Madsen, I. C.; Smith, P. W. *J. Solid State Chem.* **1987**, *69*, 162.
(15) Stranger, R.; Smith, P. W.; Grey, I. E. *Inorg. Chem.* **1989**, *28*, 1271.
(16) Dubicki, L.; Krausz, E.; Stranger, R.; Smith, P. W.; Tanabe, Y. *Inorg. Chem.* **1987**, *26*, 2247.
(17) Stranger, R. *Chem. Phys. Lett.* **1989**, *157*, 472.
(18) Stranger, R.; Moran, G.; Krausz, E.; Dubicki, L.; Güdel, H.; Furer, N. *Inorg. Chem.* **1992**, *31*, 2860.
(19) Stranger, R.; Moran, G.; Krausz, E.; Medley, G. *Inorg. Chem.* **1993**, *32*, 4555.
(20) Stranger, R. *Inorg. Chem.* **1990**, *29*, 5231.

0020-1669/94/1333-3976$04.50/0

The structures of $Cs_3Mo_2Cl_9$, $Cs_3Mo_2Br_9$, and $Cs_3Mo_2I_9$ are known,[14] and their ground-state exchange coupling constants J_{ab} have been determined from temperature-dependent magnetic susceptibility measurements.[15] The reported $-J_{ab}$ values for the chloro, bromo, and iodo complexes are 415, 380, and 475 cm^{-1}, respectively, while the corresponding metal–metal distances are 2.66, 2.82, and 3.07 Å. In addition to the Cs salts, the structures and J_{ab} values for the chloride complexes $A_3Mo_2Cl_9$ (A = K, Rb, NH_4, Me_4N) and the bromide complex $(Me_4N)_3Mo_2Br_9$ are also known.[14,15] The 35-cm^{-1} decrease in $-J_{ab}$ for the bromide complex $Cs_3Mo_2Br_9$ in relation to $Cs_3Mo_2Cl_9$ is consistent with the 0.16-Å increase in metal–metal distance, but unless substantial superexchange or other antiferromagnetic effects are operative, the rather large $-J_{ab}$ value reported for the iodide complex $Cs_3Mo_2I_9$ is unexpected considering the large increase of 0.41 Å in metal–metal distance relative to the chloride complex.

Although the electronic structure of $Mo_2Cl_9^{3-}$ has been previously investigated by both extended Hückel[21] and SCF–Xα–SW calculations,[22] no calculations have been reported on the corresponding bromide and iodide complexes. Consequently, the desire to compare the bonding in the series $Cs_3Mo_2X_9$ (X = Cl, Br, I), and to account for the unusually large $-J_{ab}$ value for the iodide complex prompted us to investigate the ground-state electronic structure and metal–metal bonding in these three complexes and, through use of the Xα–VB method, to calculate the exchange coupling constant in each case. Furthermore, the magneto–structural data available for the chloride complexes in particular provide an excellent opportunity to assess the reliability of the Xα–VB method in modeling observed magneto–structural correlations in strongly coupled dimer systems.

Experimental Section

Spin-restricted self-consistent-field Xα scattered wave (SCF–Xα–SW)[2-5] and spin-unrestricted broken-symmetry SCF–Xα–SW (alternatively Xα–VB) calculations[7,8] were performed on a DEC 5000/240 work station using a modified version of the XASW Fortran program written by Cook and Case.[23] Geometries for $Cs_3Mo_2Cl_9$ and $Cs_3Mo_2Br_9$ were taken from the reported single-crystal structures,[24] whereas those for the complexes $A_3Mo_2Cl_9$ (A = K, Rb, Me_4N), $(Me_4N)_3Mo_2Br_9$, and $Cs_3Mo_2I_9$ were obtained from the reported rietveld structure refinement of powder X-ray diffraction data.[14] Unless otherwise specified, the atomic sphere radii were chosen using the Norman criteria.[25,26] Additional broken-symmetry Xα–SW calculations were performed with the sphere radii for Mo reduced to 1.184 and 1.380 Å for $Cs_3Mo_2Cl_9$ and $Cs_3Mo_2Br_9$, respectively, in order to fit the calculated J_{ab} values to those observed experimentally. Further calculations for the K, Rb, and Me_4N salts were undertaken by adjusting the Mo sphere radii in proportion to their metal–metal bond lengths relative to the Cs salts. The α values used in the atomic regions were those determined by Schwartz,[27,28] while those used in the inter-atomic and outer-sphere regions were atomic number weighted averages of the atomic α values. In order to impose the spin-up and spin-down mirror symmetry on opposite sides of the dimer required in the spin-unrestricted broken-symmetry Xα–SW calculations, initial spin-polarized atomic potentials for Mo^{3+} were constructed with three spin-up and three spin-down electrons in the 4d orbitals, while the SCF refinements were carried out in C_{3v} molecular symmetry in order to remove symmetry operations connecting the two halves of the dimer. The wave functions were expanded in spherical harmonics out to $l = 5$ on the outer-sphere, $l = 2$ on the Mo atoms, and $l = 1$ on the Cl atoms. A Watson sphere of 3+ charge coincident with the outer-sphere radius was used to account for the negative charge of the complexes. Transition energies within the ground-state spin manifold were determined using the Slater transition state method.[2]

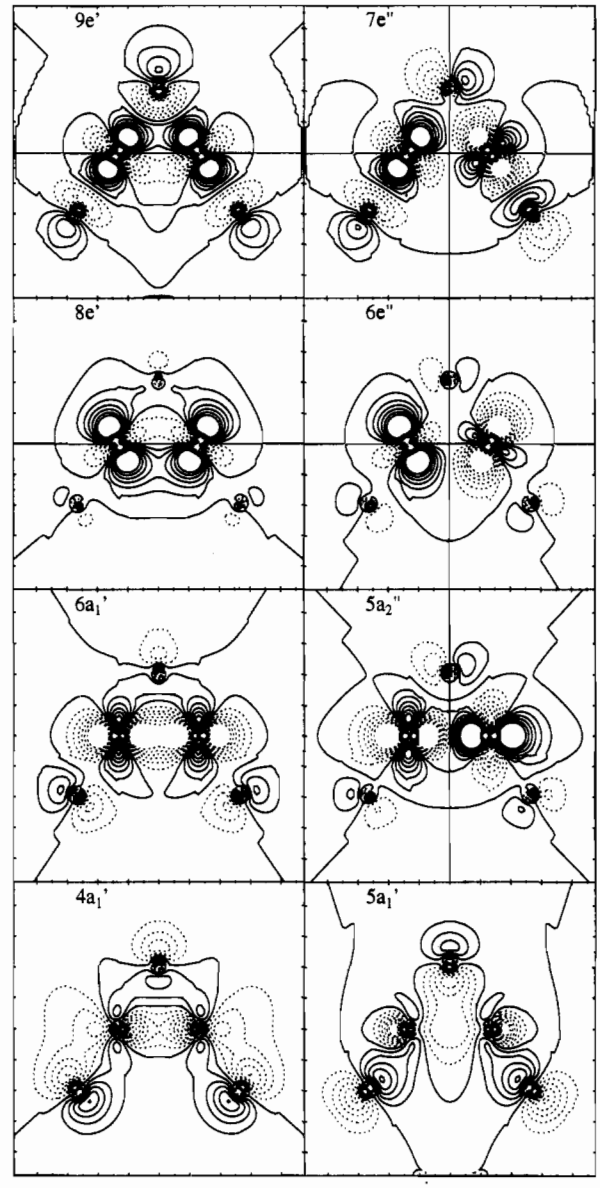

Figure 1. Contour plots in the (Cl_t–Mo–Cl_b–Mo–Cl_t) plane of the spin-restricted wave functions for the valence molecular orbitals in $Cs_3Mo_2Cl_9$ which comprise significant Mo–Mo bonding or antibonding contributions. Solid and broken lines indicate positive and negative signs of the wave function, respectively. Contour intervals correspond to 0, ±0.02, ±0.04, ±0.06, ±0.08, ±0.10, and ±0.12 (electrons/$Bohr^3)^{1/2}$.

Results and Discussion

1. Ground-State Spin-Restricted Xα–SW Calculations. The ground-state valence energy levels, charge distributions, and orbital descriptions for $Cs_3Mo_2Cl_9$, $Cs_3Mo_2Br_9$, and $Cs_3Mo_2I_9$ are detailed in Table 1. Contour maps of orbitals containing significant amounts of Mo–Mo bonding or antibonding character for $Cs_3Mo_2Cl_9$ are shown in Figure 1.

Since the valence energy level pattern for all three halide complexes is similar, only the chloride complex will be described in detail. For the chloride complex, the valence levels can be grouped more or less into eight categories in order of increasing energy: (1) two nonbonding Cl_b 3s orbitals ($1a_1'$, $1e'$); (2) four nonbonding Cl_t 3s orbitals ($1a_2''$, $2a_1'$, $2e'$, $1e''$); (3) two orbitals ($3e'$,$2e''$) comprising both Mo–Cl_b and Mo–Cl_t bonding character; (4) six orbitals ($3a_1'$, $2a_2''$, $4e'$, $5e'$, $6e'$, $4a_2''$) comprising both Cl_b and Cl_t 3p nonbonding character; (5) nine Cl_t 3p nonbonding orbitals ($3e''$, $3a_2''$, $4a_1'$, $5a_1'$, $4e''$, $1a_1''$, $7e'$, $5e''$, $2a_2'$); (6) one

(21) Summerville, R. H.; Hoffmann, R. J. *J. Am. Chem. Soc.* **1979**, *101*, 3821.
(22) Ginsberg, A. P. *J. Am. Chem. Soc.* **1980**, *102*, 111.
(23) Cook, M.; Case, D. A. XASW-A Fortran Program for Atomic X-Alpha and Molecular Multiple Scattering X-Alpha Electronic Structure Calculations, Version 2. QCPE Program 465, 1982.
(24) Saillant, R.; Jackson, R. B.; Streib, W. E.; Folting, K.; Wentworth, R. A. D. *Inorg. Chem.* **1971**, *10*, 1453.
(25) Norman, J. G., Jr. *J. Chem. Phys.* **1974**, *61*, 4630.
(26) Norman, J. G., Jr. *Mol. Phys.* **1976**, *31*, 1191.
(27) Schwarz, K. *Phys. Rev. B* **1972**, *5*, 2466.
(28) Schwarz, K. *Theor. Chim. Acta* **1974**, *34*, 225.

Table 1. Results of the Spin-Restricted SCF–Xα–SW Calculations for $Cs_3Mo_2X_9$ (X = Cl, Br, I)

					distribution (%)								
		energy (eV)			$Cs_3Mo_2Cl_9$			$Cs_3Mo_2Br_9$			$Cs_3Mo_2I_9$		
level	orbital description	$Cs_3Mo_2Cl_9$	$Cs_3Mo_2Br_9$	$Cs_3Mo_2I_9$	Mo	Cl_b	Cl_t	Mo	Br_b	Br_t	Mo	I_b	I_t
9e′	MoX_b MoX_t antibonding	−2.225 15	−2.310 79	−2.184 04	53	13	16	51	14	17	46	16	18
7e″	MoX_b MoX_t antibonding	−2.572 09	−2.792 72	−2.886 26	58	6	18	55	8	20	46	12	23
$5a_2''$	Mo–Mo σ antibonding	−3.260 75	−3.514 44	−3.697 77	77	5	5	78	6	5	77	8	4
6e″	Mo–Mo π antibonding	−4.238 26	−4.339 53	−4.443 92	80	2	9	79	1	10	76	1	14
8e′	Mo–Mo π bonding	−4.739 04	−4.611 16	−4.520 08	72	8	9	72	8	8	68	11	9
$6a_1'$	Mo–Mo σ bonding	−5.827 78	−5.435 73	−5.097 95	68	4	19	65	5	20	57	6	26
$2a_2'$	X_t 3p nonbonding	−7.081 06	−6.380 81	−5.596 35		18	81		18	81		21	78
5e″	X_t 3p nonbonding	−7.096 92	−6.403 41	−5.639 26		17	82		14	84	1	12	86
7e′	X_t 3p nonbonding	−7.211 26	−6.518 07	−5.753 04		16	82		15	84	1	16	82
$4a_2''$	X_b X_t 3p nonbonding	−7.278 67	−6.556 59	−5.688 713	1	39	57	2	36	59	2	32	62
$1a_1''$	X_t 3p nonbonding	−7.284 08	−6.586 82	−5.849 91			99			99			99
6e′	X_b X_t 3p nonbonding	−7.590 81	−6.871 66	−6.043 32	2	34	60	2	32	62	4	27	66
4e″	X_t 3p nonbonding	−7.878 52	−7.213 05	−6.514 31	5	17	75	7	14	76	10	11	76
$1a_2'$	X_b 3p nonbonding	−8.034 46	−7.342 64	−6.626 65		81	18		81	18		78	20
$5a_1'$	X_t 3p nonbonding	−8.099 63	−7.504 86	−6.828 94	14	19	63	21	10	66	27	3	64
5e′	X_b X_t 3p nonbonding	−8.208 50	−7.556 66	−6.791 67	8	28	62	9	24	66	9	19	70
$4a_1'$	X_t 3p nonbonding	−8.532 51	−7.833 12	−7.070 4	15	13	70	12	15	70	10	13	73
$3a_2''$	X_t 3p nonbonding	−8.581 17	−7.936 70	−7.182 84	11	14	83	12	6	80	12	4	81
3e″	X_t 3p nonbonding	−8.781 35	−8.104 68	−7.338 63	14	16	67	16	13	78	20	8	69
4e′	X_b X_t 3p nonbonding	−9.081 67	−8.431 38	−7.840 05	16	50	31	18	51	29	19	49	27
2e″	MoX_b MoX_t bonding	−9.369 75	−8.697 23	−8.139 8	29	33	34	31	39	25	34	44	16
$2a_2''$	X_b X_t 3p nonbonding	−9.467 50	−8.935 83	−8.385 37	15	43	38	17	42	38	19	44	34
$3a_1'$	X_b X_t 3p nonbonding	−9.600 37	−9.128 54	−8.519 76	20	50	28	21	53	23	36	45	14
3e′	MoX_b MoX_t bonding	−9.983 95	−9.230 80	−8.566 12	33	38	25	35	41	20	22	61	15
1e″	X_t 3s	−19.387 02	−18.373 06	−15.090 2	3		96	3		97	3		97
2e′	X_t 3s	−19.391 94	−18.377 45	−15.097 0	3		96	3		97	3		97
$2a_1'$	X_t 3s	−19.404 06	−18.437 28	−15.170 8	2	19	78	1	13	85	1	12	85
$1a_2''$	X_t 3s	−19.556 06	−18.549 90	−15.338 9	3		96	3		97	3		96
1e′	X_b 3s	−19.976 35	−19.060 88	−15.996 0	4	95		3	96		4	94	
$1a_1'$	X_b 3s	−20.178 17	−19.256 05	−16.328 6	4	77	18	3	83	12	6	83	12

Cl_b 3p nonbonding orbital ($1a_2'$); (7) four levels ($6a_1'$, 8e′, 6e″, $5a_2''$) containing greater than 50% Mo 4d character which are the main σ and π metal–metal bonding and antibonding molecular orbitals; (8) finally, two levels (7e″, 9e′) which are predominantly Mo–Cl_t and Mo–Cl_b antibonding in character. The orbital energies and descriptions are similar to those reported previously[22] for $Cs_3Mo_2Cl_9$ except that we calculate the Cl_b 3s and 3p nonbonding levels to be generally lower in energy than the analogous Cl_t-based orbitals, in agreement with SCF–Xα–SW calculations on $Ru_2Cl_9^{3-}$.[29]

The valence energy levels for the Cs salts of $Mo_2X_9^{3-}$ (X = Cl, Br, I) are plotted together in Figure 2. For comparative purposes, the energy levels for the bromide and iodide complexes have been adjusted so that the center of gravity between the metal–metal bonding 8e′ and antibonding 6e″ levels is the same in all three complexes. As expected, in comparison with the chloride dimer, the Mo–halide bonding and halide nonbonding levels are raised in energy for the bromide and iodide complexes relative to the barycenter between the 8e′ and 6e″ metal–metal bonding–antibonding levels. The overall energy spread of the Mo–halide bonding and halide nonbonding levels is very similar in all three complexes. However, due to the higher energy shift of these levels in the bromide and iodide complexes relative to the Mo 4d orbitals, the lower lying Mo–halide bonding orbitals contain more metal character while the upper lying metal–metal bonding and Mo–halide antibonding levels contain more halide character relative to the chloride complex.

2. Metal–Metal Bonding. The levels involved in direct metal–metal bonding interactions consist of the metal–metal σ bonding and antibonding molecular orbitals $6a_1'$ and $5a_2''$, respectively, formed by the overlap of the single ion $4d_{z^2}$ orbitals, and the metal–metal π bonding and antibonding molecular orbitals 8e′ and 6e″, respectively. The 8e′ and 6e″ levels both result from hybrid mixtures of either the $4d_{xy}$ and $4d_{yz}$ or $4d_{x^2-y^2}$ and $4d_{xz}$ single ion orbitals and, therefore, formally involve both π and δ type metal–metal bonding interactions.[21,30] Consequently, the metal–metal π bonding is not optimized in these trigonal face-shared dimers, accounting for the weakness of this interaction relative to both unsupported and bridged D_{4h} M_2L_8 dimer complexes.[1] The metal–ligand interaction is expected to complicate the simple metal–metal π and δ description for the 8e′ and 6e″ orbitals,[21,29,30] but as can be seen from the contour plots shown in Figure 1, both these orbitals are essentially of metal–metal π bonding or antibonding character. In addition to the upper valence metal–metal bonding levels responsible for the magnetic interactions between the two metal centers, two other lower lying orbitals $4a_1'$ and $5a_1'$ also contain significant metal–metal σ bonding character, as can be seen from the contour plots of these orbitals shown in Figure 1.

From an examination of Figure 2, it is clear that the metal–metal σ and π bonding–antibonding orbital separations decrease significantly in the order $Mo_2Cl_9^{3-}$, $Mo_2Br_9^{3-}$, and $Mo_2I_9^{3-}$, consistent with the increase in metal–metal distance of 0.16 and 0.41 Å for the bromide and iodide complexes, respectively, relative to the chloride complex. Overall, on the basis of these metal–metal bonding–antibonding molecular orbital separations, the metal–metal σ bond interaction in the iodide complex is reduced to around 55% of that of the chloride complex, while the reduction in the metal–metal π interaction is even greater, only 15% of the chloride interaction.

The higher lying 7e″ and 9e′ levels, which from the contour plots shown in Figure 1 are essentially Mo–halide antibonding orbitals, are also involved in direct π and δ type metal–metal interactions, although not in the ground state as these orbitals are not occupied. In Figure 2, the progressive increase in separation of the 7e″ and 9e′ molecular orbitals from the chloride to iodide complex is a result of two types of interactions. In the absence of any direct metal–metal interaction, the Mo–halide

(29) Bursten, B. E.; Cotton, A. F.; Fang, A. *Inorg. Chem.* **1983**, *22*, 2127.

(30) Trogler, W. C. *Inorg. Chem.* **1980**, *19*, 697.

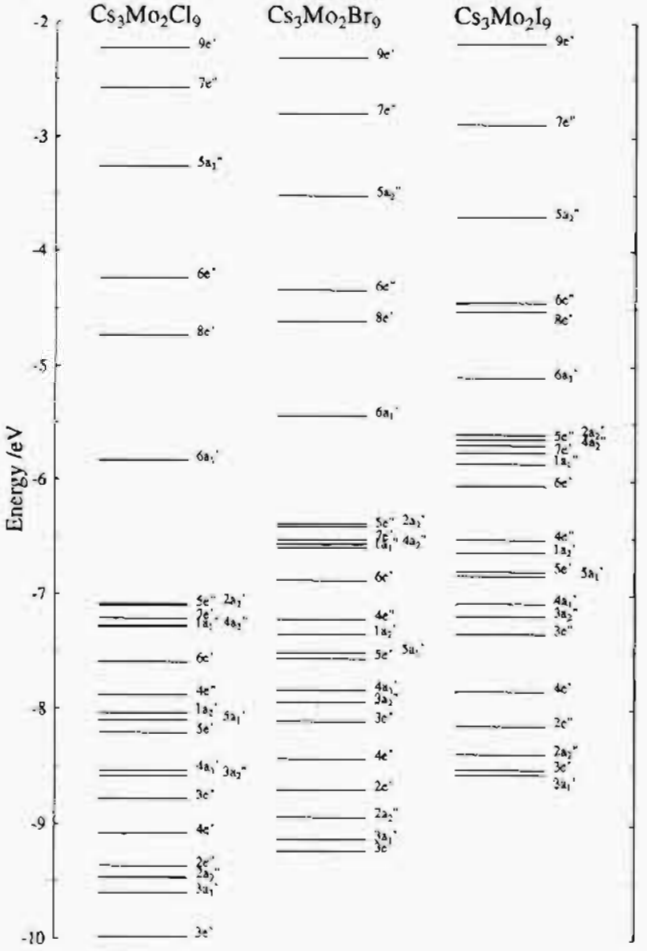

Figure 2. Spin-restricted $S = 0$ ground-state valence energy level diagrams for $Cs_3Mo_2X_9$ (X = Cl, Br, I). For comparative purposes, the energy levels for the bromide and iodide complexes have been adjusted in order to maintain a constant center of gravity between the 8e′ (HOMO) and 6e″ LUMO) levels in all three complexes. The energy levels corresponding to the bridging and terminal halide nonbonding 3s orbitals for each complex are not shown.

antibonding interaction forces the 9e′ level above the 7e″ orbital whereas the metal–metal π bonding interaction stabilizes the 9e′ orbital in preference to the 7e″ orbital. Consequently, the net separation of the 9e′ and 7e″ orbitals is a balance between these two opposing interactions. Obviously, since the 9e′ level lies to higher energy in all three complexes, the Mo–halide antibonding interaction is the dominant effect.

It is anticipated that the major contribution to the exchange interaction in $Mo_2X_9^{3-}$ complexes will be from the direct overlap of the Mo 4d orbitals. However, the problem of superexchange contributions, particularly for the iodide complex, cannot be dismissed. This problem can be addressed by examining both the contour plots and surface plots of the $6a_1'$ and 8e′ orbitals for the iodide complex shown in Figure 3, as well as the charge distributions for these two orbitals given in Table 1. If superexchange effects are operative, then it should be possible to observe some delocalization of the magnetic orbitals through overlap with the bridging halide ligands. Although a small amount of charge is certainly localized on the bridging iodide ligands for these orbitals, it is essentially nonbonding. Consequently, even for the iodide complex, the exchange interaction is almost entirely the result of direct overlap of magnetic orbitals on adjacent metal centers. The same conclusion is reached for both the chloride[22] and bromide complexes.

3. Ground-State Exchange Coupling. In the case of weakly coupled dimers with orbitally nondegenerate single-ion ground states, the exchange coupling between the two metal centers can

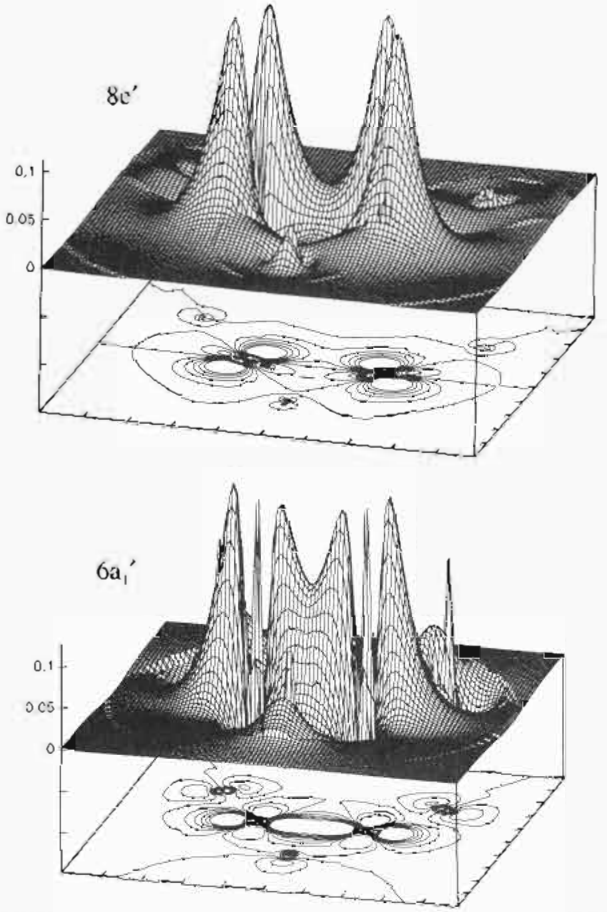

Figure 3. Surface plots of the wave functions (positive sign only) for the 8e′ and $6a_1'$ magnetic orbitals in $Cs_3Mo_2I_9$.

be described by the Heisenberg spin Hamiltonian

$$\mathcal{H}_{ex} = -2J_{ab}S_a \cdot S_b \tag{1}$$

where S_a and S_b are the single-ion spins on centers a and b, respectively, and J_{ab} is the exchange coupling constant defined by

$$J_{ab} = \sum_{ij} \frac{J_{ij}}{4S_aS_b} \tag{2}$$

Thus, J_{ab} represents the average value obtained from summing over all possible exchange pathways which are parameterized by the orbital-dependent exchange parameters J_{ij}. From $\mathcal{H}_{ex}$, the energies of the ground-state spin levels are given by

$$E(S) = -J_{ab}S(S+1) \tag{3}$$

We have previously shown[15] that when one or more of the exchange pathways corresponds to a moderate to strong metal–metal bonding interaction, the off-diagonal exchange coupling can lead to extensive configuration interaction between the ground-state spin levels and higher lying multiplets of the same total spin value. In this case, significant deviation from the simple Heisenberg description of the ground-state exchange coupling process can occur. Such a situation is known to exist in the $Mo_2Cl_9^{3-}$ and $Mo_2Br_9^{3-}$ dimer complexes since, from detailed spectroscopic studies,[16-19] the metal–metal σ bonding interaction has been shown to be quite strong, resulting in a partial pairing off of the single ion trigonal t_{2z} electrons into a metal–metal σ bond. The metal–metal π interaction on the other hand has been shown to be much weaker and effectively determines the exchange coupling splitting observed in the excited-state multiplets.

The effect of a significant metal–metal σ interaction, parametrized by J_σ, on the ground-state spin levels is shown graphically

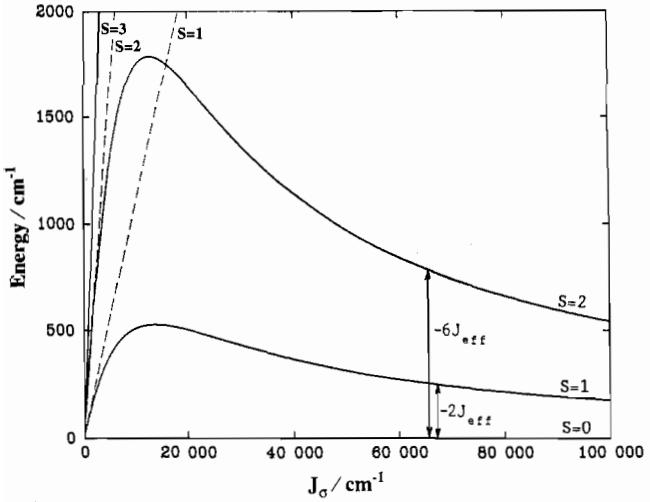

Figure 4. Energy dependence of the $t_2^3t_2^3$ ground-state pair spin levels on the metal–metal σ exchange interaction parametrized by J_σ (see refs 16 and 20 for details of calculation). The energies of the S = 1–3 spin levels are plotted relative to the S = 0 spin state. Dashed lines correspond to the energies of the spin levels determined from the Heisenberg spin Hamiltonian (expression (3) in text).

in Figure 4. In this diagram, the energies of the ground-state spin levels, determined from diagonalizing the complete $t_2^3t_2^3$ pair configuration for both the single-ion and exchange interaction Hamiltonians, are plotted as a function of J_σ. The procedure for undertaking this type of calculation has been fully detailed in previous publications.[16,20] In the present case, the single-ion ligand-field parameters have been set to those determined[15] for $MoCl_6^{3-}$ corresponding to B = 467 cm^{-1}, $C = 4B$, and Δ = 19 200 cm^{-1}, where Δ is the separation between the single-ion trigonally adapted t_{2g} and e_g orbitals. For comparison, the energies of the ground-state spin levels determined from the simple Heisenberg spin Hamiltonian are also plotted (dashed lines). Clearly, as J_σ increases, there is a corresponding increase in the energies of the S = 1–3 spin levels relative to the S = 0 spin state. However, departure from the simple Heisenberg model is evident even for J_σ around 2000 cm^{-1} as the energies of the S = 1, 2 spin levels are no longer linearly dependent on J_σ. In fact, the S = 1, 2 spin-state energies reach a maximum around J_σ = 15 000 cm^{-1} (corresponding to $-J_{ab}$ = 1665 cm^{-1} in the absence of other exchange interaction pathways) and then slowly converge to zero energy as J_σ approaches ∞. The S = 3 spin level on the other hand, although factored out to higher energy, remains approximately linearly dependent on J_{ab} and, therefore, for moderate to large J_σ, is the only ground-state spin level to be correctly described by the Heisenberg spin Hamiltonian.

From Figure 4, it is apparent that for J_σ > 2000 cm^{-1} the energies of the ground-state S = 1, 2 spin levels no longer obey a simple Heisenberg description. Furthermore, the value of J_{ab} determined from the separation of the singlet–triplet spin levels where

$$-2J_{ab} = E(S = 1) - E(S = 0) \qquad (4)$$

cannot be used to measure the extent of metal–metal interaction. For instance, at J_σ = 100 000 cm^{-1} in Figure 4, corresponding to a very strong metal–metal interaction, the observed singlet–triplet separation of approximately 250 cm^{-1} (i.e. $-J_{ab}$ = 125 cm^{-1}) would seemingly indicate a relatively weak metal–metal interaction if the Heisenberg description is assumed to apply. Perhaps even more disturbing is the fact that, initially, a weakening of the metal–metal bonding interaction can result in an increased ground-state singlet–triplet separation. This effect may possibly explain the anomalously large $-J_{ab}$ value of 475 cm^{-1} for $Cs_3Mo_2I_9$ compared to 415 cm^{-1} for the chloride complex. The 0.41-Å increase in bond distance in the iodide complex relative to $Cs_3Mo_2Cl_9$ undoubtedly results in a significant weakening of the metal–metal σ bond such that the two electrons involved in the metal–metal σ interaction may now contribute strongly to the ground-state exchange coupling, resulting in an increased singlet–triplet separation and, consequently, a larger effective $-J_{ab}$ value. However, as shown later from the Xα–VB calculations, the larger $-J_{ab}$ value for $Cs_3Mo_2I_9$ arises from ligand → metal spin-polarization effects.

The breakdown of the Heisenberg spin Hamiltonian description of the ground-state spin levels is due to the fact that the single-ion spins S_a and S_b are no longer good quantum numbers when one or more of the possible exchange pathways are involved in moderate to strong metal–metal bonding interactions. In the case of d^3d^3 dimer systems with a strong metal–metal σ interaction, applicable to the $Mo_2X_9^{3-}$ complexes, the single-ion spins will take on effective values ranging from $S_a = S_b = {}^3/_2$ in the weakly coupled case (no metal–metal bonding) through to $S_a = S_b = 1$ in the metal–metal σ bond limit. It is apparent from Figure 4 that even though the Heisenberg description of the ground-state spin levels breaks down as J_σ increases, the S = 0, 1, 2 spin levels still continue to obey an approximate Landé interval separation given by

$$E(S) = -2J_{eff}S(S + 1) \qquad (5)$$

where J_{eff} is an effective exchange coupling constant which can only be equated with the Heisenberg type J_{ab} in either the d^3d^3 weakly coupled or d^2d^2 metal–metal σ bond limits.

4. Broken-Symmetry Xα–SW Calculations. Broken symmetry Xα–SW calculations using the Xα–valence bond (Xα–VB) method, developed by Noodleman,[7,8] allow valence bond concepts to be incorporated into the Xα formalism. This approach has been quite successful in the calculation of ground-state exchange coupling constants for a number of Cu(II) dimers,[9-12] binuclear iron–sulfur complexes and iron–sulfur cluster compounds,[13,31-35] and very recently in a mixed chloro–thioether face-shared dimer complex of Mo(III).[36] In this approach, the dimer is considered initially as two equivalent interacting monomeric subunits but with the unpaired (magnetic) electrons on each fragment having opposite spin. By introduction of this spin-inversion symmetry between the metal centers, additional electron correlation is achieved over and above that present in the normal Xα method.

In the ground state Xα–VB calculation, the self-consistent-field (SCF) procedure allows the magnetic orbitals on each subunit to interact resulting in a state of mixed spin symmetry and lowered space symmetry referred to as the broken-symmetry state. The energy of this broken-symmetry state is a weighted average of all possible ground-state spin multiplets arising from the exchange interaction between the two metal centers. The results of the broken-symmetry ground-state SCF–Xα–SW calculations on $Cs_3Mo_2X_9$ (X = Cl, Br, I) in C_{3v} symmetry are detailed in Table 2. In addition, the energy level diagram for the antiferromagnetic broken-symmetry ground state of $Cs_3Mo_2Cl_9$ is shown in Figure 5. In this diagram, the orbital energies are plotted as a function of their % localization on the left or right side of the dimer. The orbitals are also grouped according to their spin polarization with spin-up (↑) orbitals shown in solid lines and spin-down (↓) orbitals shown in dashed lines. Because of the spin inversion symmetry existing between opposite halves of the molecule, each spin-up

(31) Norman, J. G., Jr.; Ryan, P. B.; Noodleman, L. *J. Am. Chem. Soc.* **1980**, *102*, 4279.
(32) Aizman, A.; Case, D. A. *J. Am. Chem. Soc.* **1982**, *104*, 3269.
(33) Noodleman, L.; Norman, J. G., Jr.; Osborne, J. H.; Aizman, A.; Case, D. A. *J. Am. Chem. Soc.* **1985**, *107*, 3418.
(34) Noodleman, L.; Case, D. A.; Aizman, A. *J. Am. Chem. Soc.* **1988**, *110*, 1001.
(35) Noodleman, L.; Case, D. A. *Adv. Inorg. Chem.* **1992**, *38*, 423.
(36) Jacobsen, H.; Kraatz, H. B.; Ziegler, T.; Boorman, P. M. *J. Am. Chem. Soc.* **1992**, *114*, 7851.

Table 2. Results of the Broken-Symmetry SCF–Xα–SW Calculations for $Cs_3Mo_2X_9$ (X = Cl, Br, I)

		charge distribution (%)											
		Mo (L)			Mo (R)			X_b		X_t (L)		X_t (R)	
level	energy (eV)	s	p	d	s	p	d	s	p	s	p	s	p
					$Cs_3Mo_2Cl_9$								
16e↓	−1.424 68		1	69				6	6	7	11		
16e↑	−1.424 68					1	69	6	6			7	11
15e↓	−2.753 00			1		1	62	3	9			6	18
15e↑	−2.753 00		1	62			1	3	9	6	18		
$11a_1$↓	−3.169 21			68	1	1	21		5		3		1
$11a_1$↑	−3.169 21	1	1	21			68		5		1		3
14e↓	−3.856 76			89			2		3		6		
14e↑	−3.856 76			2			89		3				6
13e↓	−5.559 69			1			79		6				13
13e↑	−5.559 69			79			1		6		13		
$10a_1$↓	−6.221 77			18			53		6		6		16
$10a_1$↑	−6.221 77			53			18		6		16		6
					$Cs_3Mo_2Br_9$								
16e↓	−1.582 12			67				7	7	7	11		
16e↑	−1.582 12						67	7	7			7	11
15e↓	−2.988 30			1		1	56	3	12		1	6	21
15e↑	−2.988 30		1	56			1	3	12	6	21		1
$11a_1$↓	−3.387 20			76		1	14		5		4		1
$11a_1$↑	−3.387 20		1	14			76		5		1		4
14e↓	−3.795 30			91			1		3		6		
14e↑	−3.795 30			1			91		3				6
13e↓	−5.574 26						75		6		1		17
13e↑	−5.574 26			75					6		17		1
$10a_1$↓	−5.897 19			11			55		8		7		19
$10a_1$↑	−5.897 19			55			11		8		19		7
					$Cs_3Mo_2I_9$								
16e↓	−2.194 32			65			1	6	9	6	12		1
16e↑	−2.194 33			1			65	6	9		1	6	12
15e↓	−3.615 61			4			48	2	16		1	4	25
15e↑	−3.615 61			48			4	2	16	4	25		1
$11a_1$↓	−4.256 07			82			8		6		4		
$11a_1$↑	−4.256 07			8			82		6				4
14e↓	−4.510 54			90			1		3		6		1
14e↑	−4.510 54			1			90		3		1		6
13e↑	−6.252 23			63					7		25		5
13e↓	−6.252 24						63		7		5		25
$10a_1$↓	−6.314 24			4			48		11		15		21
$10a_1$↑	−6.314 24			48			4		11		21		15

level on the left is energetically degenerate with an equivalent spin-down level on the right. The highest occupied levels (HOMO) correspond to the 13e↑ and 13e↓ orbitals localized on the left and right sides of the molecule, respectively. These, plus the $10a_1$↑ and $10a_1$↓ orbitals, are the magnetic orbitals involved in the exchange interaction between the two metal ions.

Large spin-polarization effects are also evident for these magnetic orbitals with the spin-up orbitals strongly stabilized with respect to the analogous spin-down orbitals for the left side of the dimer while the reverse order applies for the right side. For instance, spin-polarization is responsible for the ~1.7-eV splitting observed between the 13e↑ and 14e↓ orbitals on the left side of the dimer (see Table 2). In a spin-restricted calculation these levels would be degenerate, and in the D_{3h} molecular-orbital scheme these levels comprise the orbitals which participate in the metal–metal π exchange interaction. The splitting arising from spin-polarization effects is greatest for the $10a_1$↑ and $11a_1$↓ levels (~3.0 eV) which are involved in the metal–metal σ exchange interaction. In general, spin-polarization effects produce much smaller splittings of less than 1 eV for orbitals largely localized on either the bridging or terminal chlorides. Overall, the spin-polarization effects were found to increase for the bromide and iodide complexes relative to $Mo_2Cl_9^{3-}$, with the largest splittings found for the iodide complex.

The extent of localization of the magnetic orbitals is evident from the charge distributions given in Table 2 as well as the contour plots and surface plots of these orbitals for the chloride complex shown in Figures 6 and 7. Clearly, with 53% and 18% of charge localized at the metal on the left and right, respectively, for the $10a_1$↑ level in $Mo_2Cl_9^{3-}$, and similarly 68% and 21% for the $11a_1$↓ level, both of these orbitals are significantly delocalized

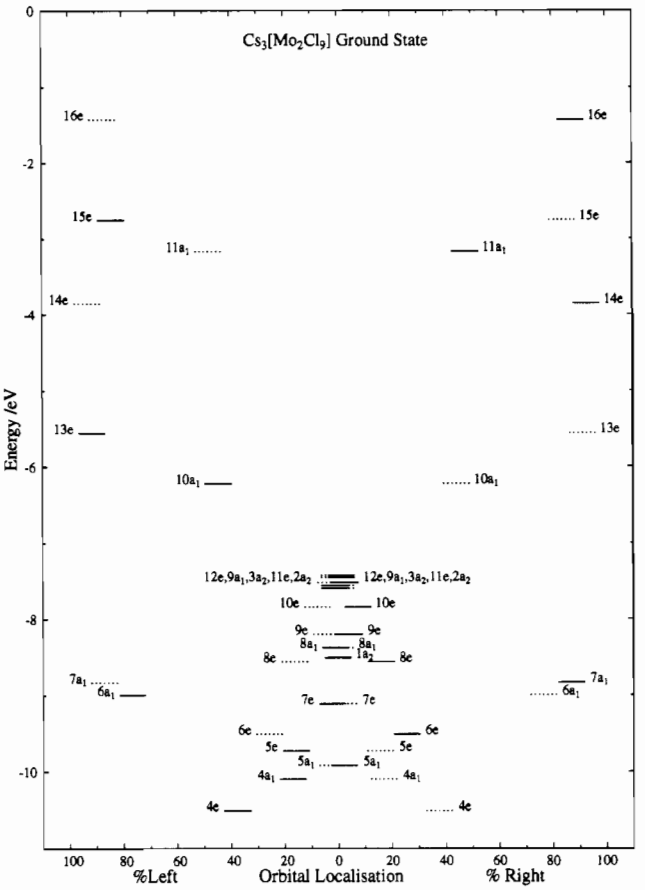

Figure 5. Broken-symmetry ground-state energy level diagram for $Cs_3Mo_2Cl_9$ showing the % localization of the levels on either the left or right side of the dimer. The % localization is defined as [(Mo(R) + Cl_t(R)) − (Mo(L) + Cl_t(L))]%. Spin-up (↑) and spin-down (↓) levels are shown in solid and dashed lines, respectively. The HOMO corresponds to the 13e↑ and 13e↓ levels. The energy levels corresponding to the bridging and terminal chloride nonbonding 3s orbitals are not shown.

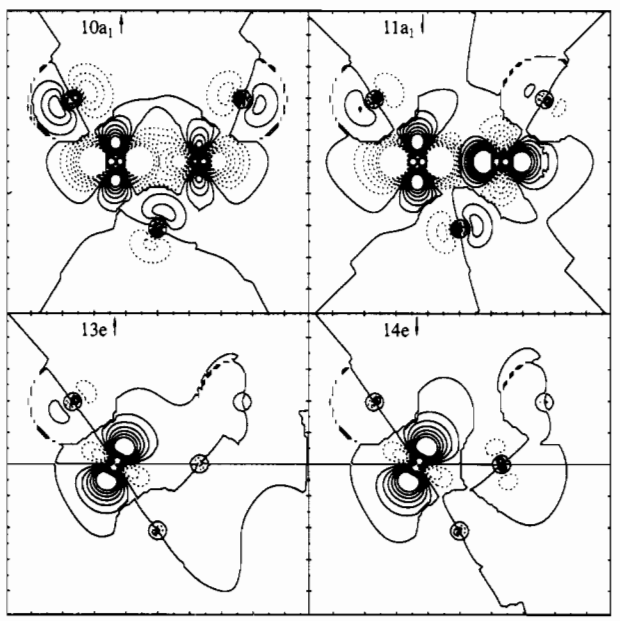

Figure 6. Broken-symmetry contour maps in the (Cl_t–Mo–Cl_b–Mo–Cl_t) plane showing the extent of delocalization between the left and right halves of the dimer for the $10a_1$↑, $11a_1$↓, 13e↑, and 14e↓ magnetic orbitals in $Cs_3Mo_2Cl_9$. Contour intervals correspond to 0, ±0.02, ±0.04, ±0.06, ±0.08, ±0.10, and ±0.12 (electrons/$Bohr^3)^{1/2}$.

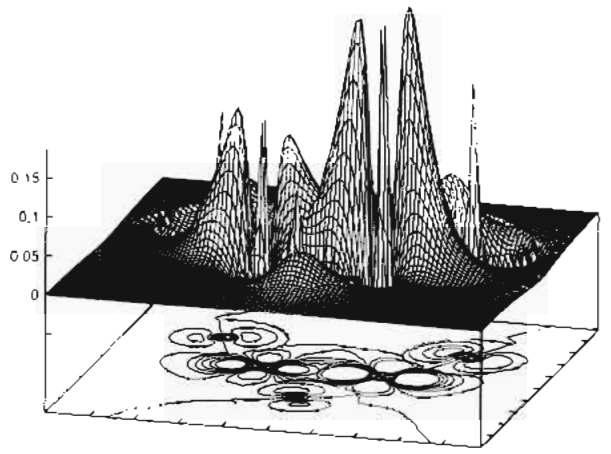

Figure 7. Surface plot of the wavefunction (positive sign only) for the $11a_1\uparrow$ broken-symmetry magnetic orbital in $Cs_3Mo_2Cl_9$ showing the extent of delocalization between the left and right halves of the dimer.

between the two metal centers as a result of the relatively strong metal–metal σ interaction. In contrast, the highly asymmetric charge distribution of 79% and 1% at the metal on the left and right, respectively, for the $13e\uparrow$ level, and similarly 89% and 2% for the $14e\downarrow$ level, indicate that these two magnetic orbitals are essentially localized on the metal centers, a consequence of the much weaker metal–metal π interaction. In the iodide complex, only 48% and 4% of charge is localized at the metal on the left and right, respectively, for the $10a_1\uparrow$ orbital. Therefore, the extent of delocalization of the σ magnetic orbitals in $Mo_2I_9^{3-}$ is much smaller than for the chloride complex, indicating a substantial weakening of the metal–metal σ bond. Not unexpectedly, the delocalization of this orbital in $Mo_2Br_9^{3-}$ is intermediate between the chloride and iodide complexes. In order to highlight the differing extent of delocalization of the magnetic orbitals in these three complexes, their energies are plotted as a function of the % localization on the left or right metal center of the dimer in Figure 8.

Noodleman[8] has shown that in the weakly coupled case, where the overlap of magnetic orbitals on adjacent metal centers is small, the exchange coupling constant J_{ab} is related to the difference between the energy of the highest spin multiplet $E(S_{max})$ and the energy of the broken-symmetry ground state E_B through

$$-J_{ab} = \frac{[E(S_{max}) - E_B]}{S^2_{max}} \qquad (6)$$

In the strongly coupled case, where the magnetic orbitals are effectively delocalized over both metal centers, the broken-symmetry ground state will correspond to the dimer $S = 0$ spin state determined from a spin-unrestricted D_{3h} calculation, and therefore, from expressions (3) and (4) one obtains

$$-J_{ab} = \frac{E(S_{max}) - E_B}{S_{max}(S_{max} + 1)} \qquad (7)$$

In both the weakly coupled and strongly coupled cases, the energy difference between the broken-symmetry ground state and the highest lying spin multiplet can be calculated using the Slater transition-state method.[2] The calculated J_{ab} values using expressions (6) and (7) will differ only by a factor $S^2_{max}/(S^2_{max} + S_{max})$, corresponding to $^2/_3$ and $^3/_4$, respectively, for $S_{max} = 2$ and $S_{max} = 3$.

As already discussed, a complication arises for $Mo_2X_9^{3-}$ complexes in that the strong metal–metal σ bonding interaction may effectively factor out some of the contribution of the σ electrons to the ground-state exchange coupling process. In this case, as far as the magnetic electrons are concerned, the maximum

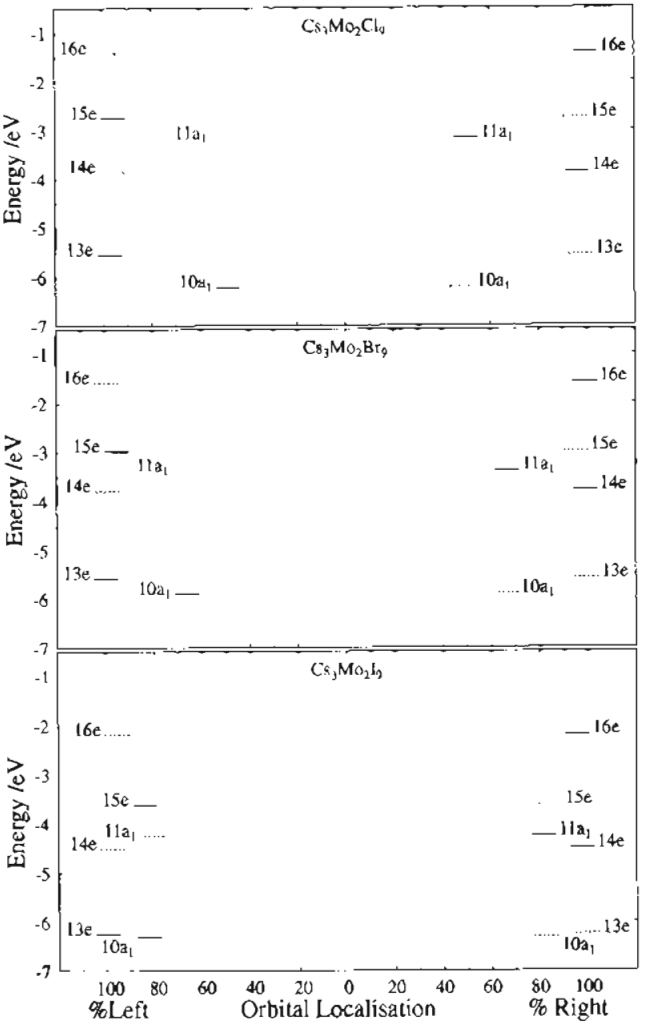

Figure 8. Broken-symmetry ground-state energy level diagrams of the magnetic orbitals in $Cs_3Mo_2X_9$ (X = Cl, Br, I) showing the % localization of the levels on either the left or right metal center of the dimer. The % localization is defined as $[(Mo(R) - Mo(L))/(Mo(R) + Mo(L))] \times 100\%$. Spin-up (↑) and spin-down (↓) levels are shown in solid and dashed lines, respectively. The HOMO corresponds to the $13e\uparrow$ and $13e\downarrow$ levels.

spin state will lie between $S_{max} = 2$ and $S_{max} = 3$. Furthermore, due to the breakdown of the Heisenberg description of the ground-state spin levels, the value of $-J_{ab}$ determined from the $S_{max} = 3$ spin state will not correspond to twice the energy of the spin singlet–triplet separation. Consequently, the value of $-J_{ab}$ obtained from the broken-symmetry Xα–SW calculations with $S_{max} = 3$ will be larger than the real spin singlet–triplet separation and at most can only be viewed as an upper limit for the true value of J_{ab}. Strictly speaking, neither eq 6 or 7 is theoretically valid in the present case as not all electrons are either weakly or strongly coupled. In the weakly coupled $S_{max} = 2$ case, the contribution of the metal–metal-based σ electrons to the ground-state exchange coupling is ignored while in the strongly coupled $S_{max} = 3$ case, the magnetic electrons involved in the metal–metal π interaction are assumed to be strongly coupled, which, on the basis of Table 2 and Figures 5 and 6, is clearly not justified. However, it is reasonable to assume that the calculated value of J_{ab} should lie between these two limits.

In order to calculate the ground-state exchange coupling constants J_{ab} for the $Mo_2X_9^{3-}$ (X = Cl, Br, I) complexes, use is made of the Slater transition-state method[2] to determine the energy difference between the maximum spin-state multiplet and the broken-symmetry ground state as required in expressions (6) and (7). For the $S_{max} = 3$ case in which the metal–metal σ electrons are assumed to contribute to the ground-state exchange interaction, the transition state is formed by removing half an

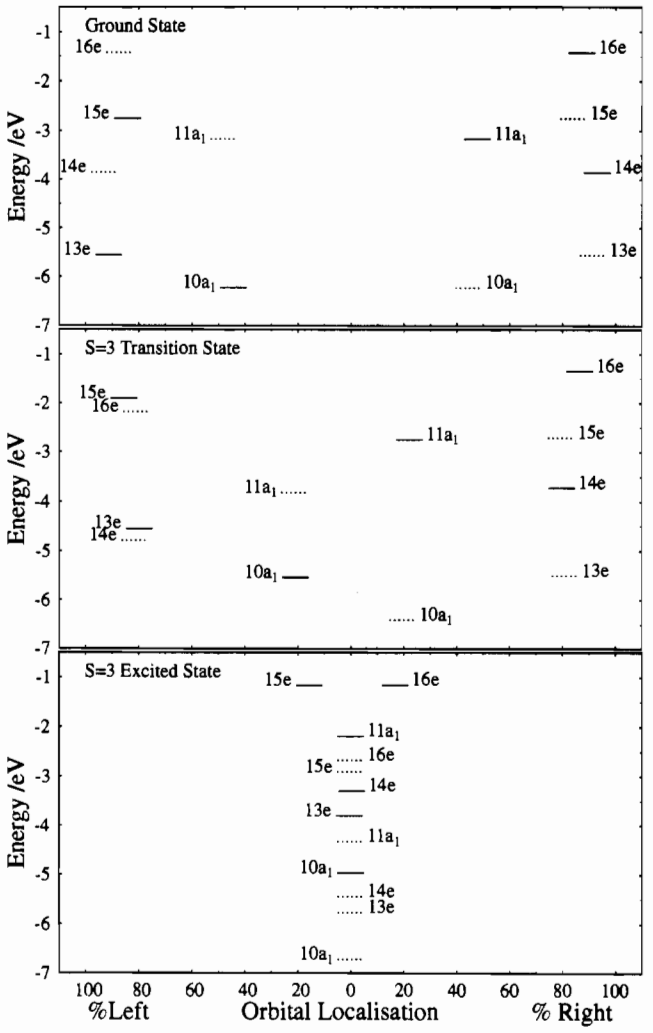

Figure 9. Energy level diagrams of the magnetic orbitals in the broken-symmetry ground state and $S_{max} = 3$ transition and excited spin states in $Cs_3Mo_2Cl_9$ showing the % localization of the levels on either the left or right side of the dimer. The % localization is defined as $[(Mo(R) + Cl_t(R)) - (Mo(L) + Cl_t(L))]\%$. Spin-up (↑) and spin-down (↓) levels are shown in solid and dashed lines, respectively.

Table 3. Exchange Coupling Constants Determined from Broken-Symmetry SCF-Xα-SW Calculations for $Cs_3Mo_2X_9$ (X = Cl, Br, I)

		calcd $-J_{ab}$ (cm^{-1})			
	obsd $-J_{ab}$	$S = 2$		$S = 3$	
complex	(cm^{-1})	weak	strong	weak	strong
$Cs_3Mo_2Cl_9$	414	846.2	564.1	1125.6	844.2
$Cs_3Mo_2Br_9$	380	1212.6	808.4	578.2	433.6
$Cs_3Mo_2I_9$	467	1650.2	1100.4	215.4	161.5

electron from the $10a_1$↑ level and placing it in the $11a_1$↓ level and removing one electron from the 13e↑ level and placing it in the 14e↓ level. For the $S_{max} = 2$ case in which the metal–metal σ electrons are assumed to be factored out and therefore do not contribute to the ground-state exchange coupling, the transition state is formed by only removing one electron from the 13e↑ level and placing it in the 14e↓ level.

The calculated J_{ab} values for all three halide complexes in the weakly-coupled (expression (6)) and strongly-coupled (expression (7)) limits for both $S_{max} = 3$ and $S_{max} = 2$ are given in Table 3, while the % localization of the magnetic orbitals on the left or right side of the chloride dimer for the broken-symmetry ground state and $S_{max} = 3$ transition and excited spin states are shown in Figure 9. It is apparent from Figure 9 that almost complete delocalization of the magnetic orbitals has occurred for the chloride complex in the $S_{max} = 3$ excited state relative to the broken-symmetry ground state (the same conclusion also applies for the $S_{max} = 2$ excited state). The bromide and iodide complexes behave similarly. Even in the $S_{max} = 3$ transition state, a dramatic increase in delocalization is evident. The splitting between the 13e↑ and 14e↓, and also the $10a_1$↑ and $11a_1$↓, magnetic orbitals on the left side of the dimer is significantly reduced in both the $S_{max} = 2$ and 3 transition states and even further in the corresponding excited states due to loss of spin-polarization. In contrast, the spin-polarization splitting between the analogous orbitals on the right side is relatively unchanged from the broken-symmetry ground-state calculation. Interestingly, in all three complexes, spin-polarization effects have resulted in the 13e↑ and 14e↓ levels being inverted for the $S_{max} = 3$ case, implying a ferromagnetic contribution to J_{ab} in the $S_{max} = 3$ excited state for these levels which correspond to the orbitals involved in the metal–metal π interaction.

In the $S_{max} = 3$ case, the calculated $-J_{ab}$ values increase in the order Cl > Br > I. This trend is primarily the result of the decreasing separation between the $10a_1$↑ and $11a_1$↓ magnetic orbitals involved in the metal–metal σ interaction, as the separation between the 13e↑ and 14e↓ magnetic orbitals is relatively similar in all three complexes. This trend is in agreement with the experimentally determined J_{ab} values for the chloride and bromide complexes but not for the iodide complex. Furthermore, the reduction in $-J_{ab}$ in going from the chloride to the bromide complex is much too large compared to the experimental values. In contrast, the $-J_{ab}$ values calculated for the $S_{max} = 2$ case, where the contribution of the metal-based σ electrons is neglected, increase in the opposite order with the largest $-J_{ab}$ value calculated for the iodide complex. The reverse trend for the $S_{max} = 2$ case arises from the greater antiferromagnetic spin-polarization splitting of the 13e↑ and 14e↓ magnetic orbitals in the order Cl < Br < I. Clearly, the calculations indicate that neither the $S_{max} = 2$ or $S_{max} = 3$ case applies but rather an intermediate value of S_{max} between 2 and 3 due to the partial factoring-out of the metal–metal σ electrons. Using an appropriate intermediate S_{max} value, it is possible to model the observed trend in J_{ab} values for the chloride, bromide, and iodide complexes, but the S_{max} value required is quite sensitive to the atomic sphere radii used for Mo.

From Table 3 it is apparent that the $-J_{ab}$ values calculated for $S_{max} = 2$ are larger than those for $S_{max} = 3$ in both the bromide and iodide complexes. As indicated above, this results from the large antiferromagnetic spin-polarization splitting of the 13e↑ and 14e↓ π magnetic orbitals in the bromide and iodide complexes for $S_{max} = 2$ compared to $S_{max} = 3$. For $S_{max} = 2$, the 13e↑ level lies below the 14e↓ level and so gives rise to an antiferromagnetic contribution to J_{ab}. In contrast, for $S_{max} = 3$, the 13e↑ and 14e↓ levels are inverted leading to a ferromagnetic contribution to J_{ab} and consequently a reduction in the ground-state spin singlet–triplet energy gap. In the $S_{max} = 3$ case for the chloride complex, the much larger separation between the $10a_1$↑ and $11a_1$↓ levels associated with the metal–metal σ interaction more than compensates for the ferromagnetic contribution arising from the inversion of the 13e↑ and 14e↓ levels, and consequently, $-J_{ab}$ is larger than that calculated for $S_{max} = 2$. For the bromide and iodide complexes, the metal–metal σ interaction is substantially weaker and, consequently, the $-J_{ab}$ values for $S_{max} = 3$ are smaller than those calculated for $S_{max} = 2$.

From the above discussion, it can be concluded that the electrons involved in the metal–metal σ interaction do contribute, if only partially, to the ground-state exchange coupling. The implication here is that even for the chloride complex the metal–metal σ bond is not optimized. This finding concurs with that found from the spectroscopic analysis of $Cs_3Mo_2Cl_9$.[16-19] On the basis of the degree of localization of the σ magnetic orbitals given in Table 2, the extent to which the σ electrons are involved in the ground-state exchange coupling progressively increases for the bromide and iodide complexes relative to $Mo_2Cl_9^{3-}$.

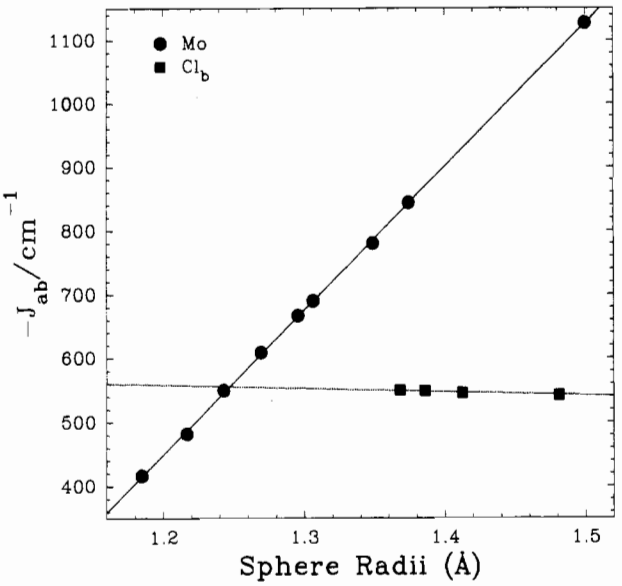

Figure 10. Plot of the variation of the ground-state exchange coupling constant $-J_{ab}$ with change in the Mo or Cl atomic sphere radii.

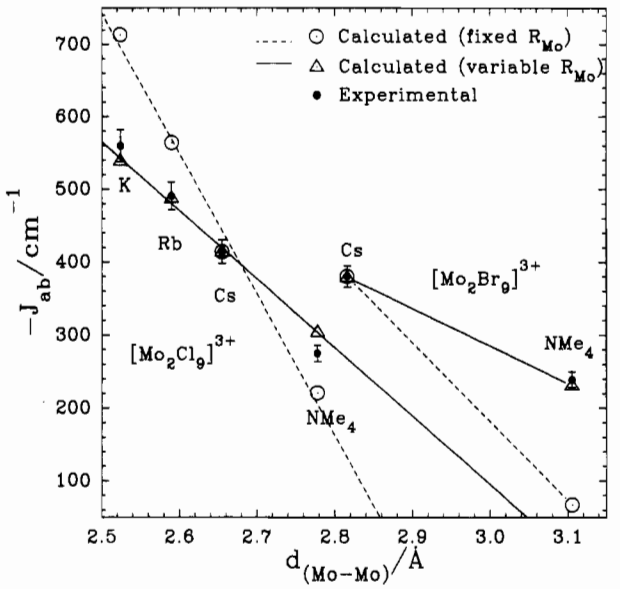

Figure 11. Plot of the experimental and calculated exchange coupling constants $-J_{ab}$ versus metal–metal distance d_{Mo-Mo} in $A_3Mo_2X_9$ (X = Cl, Br) complex salts. Experimental points are indicated by squares. Open circles indicate calculated J_{ab} values using fixed Mo atomic sphere radii of 1.184 and 1.380 Å for the chloride and bromide complexes, respectively, corresponding to the best fit to the experimental J_{ab} values for the Cs salts. Triangles correspond to calculated J_{ab} values with Mo atomic sphere radii adjusted from 1.184 and 1.380 Å for the chloride and bromide complexes, respectively, in proportion to the metal–metal distance relative to the Cs salts.

At this point it is appropriate to make some comment on the mechanism responsible for the substantial increase observed in $-J_{ab}$ of around 250 and 500 cm^{-1} for the bromide and iodide complexes, respectively, compared to the predicted $-J_{ab}$ value for the chloride complex at a similar metal–metal distance (~3.0 Å). In the past,[15,37,38] this increase in $-J_{ab}$ was attributed to antiferromagnetic superexchange effects but, as shown from the Xα–SW calculations, this effect is negligible in all three complexes. Quite recently, Daudey et al.[39] and Noodleman et al.[35,40] have shown that ligand spin-polarization effects, particularly those arising from ligand → metal single-excitations, can contribute significantly to the observed antiferromagnetic coupling. Furthermore, Noodleman and Davidson[40] have also shown that the ground-state singlet–triplet splitting calculated using the broken-symmetry method will include a reasonable estimate of this contribution. In the case of pyridine *N*-oxide–Cu(II) dimers, this term was found to contribute around 500 cm^{-1} to the calculated singlet–triplet splitting.[41] From the results of broken-symmetry calculations reported in Table 2, it is apparent that spin-polarization splitting is primarily responsible for the larger $-J_{ab}$ values determined for the bromide and iodide complexes in the $S_{max} = 2$ calculation. Consequently, on the basis of Noodleman's findings, we attribute this increase to ligand → metal based spin-polarization effects. This conclusion appears to be consistent with the larger contribution of the terminal halides to the 13e↑ and 13e↓ magnetic orbitals observed for both the bromide and iodide complexes, particularly the latter, relative to the chloride complex.

In order to model the magneto–structural correlations observed for the $A_3Mo_2Cl_9$ complexes,[15] the atomic sphere radius for Mo was adjusted until the calculated J_{ab} value for $Cs_3Mo_2Cl_9$ in the strongly coupled $S_{max} = 3$ case agreed with the experimental J_{ab} value. This corresponded to a reduced sphere radii for Mo of 1.184 Å compared to 1.375 Å calculated using the Norman criteria.[25,26] A similar approach of adjusting the metal sphere radii has been used by other workers in order to fit the experimental *g*-values or transition-state energies found for a number of Cu(II) complexes.[9,10,12,42-44] A linear dependence of the calculated J_{ab} values on the Mo sphere radii was found as shown in Figure 10. Changing the sphere radii for Cl had negligible effect on the calculated value of J_{ab} (see Figure 10), substantiating the conclusion drawn from the spin-restricted Xα–SW calculations that superexchange effects, via overlap of the magnetic orbitals with the bridging halides, do not contribute to the exchange interaction. The J_{ab} values for the K, Rb, and Me_4N salts were then calculated using this reduced sphere radii for Mo. No calculations were performed for the NH_4 salt as the structural parameters and experimental J_{ab} values are very similar to the Rb salt. An analogous procedure was employed to model the magneto–structural data observed for the Cs and Me_4N salts of the bromide complex. In this case, in order to fit the observed J_{ab} value for the Cs salt, a reduced sphere radii for Mo of 1.380 Å was used compared to 1.561 Å based on the Norman criteria. The calculated J_{ab} values for the chloride and bromide complex salts using these reduced Mo sphere radii are listed in Table 4. The experimental and calculated J_{ab} values versus metal–metal bond distance are plotted in Figure 11, and although the observed linear relationship between these parameters is reproduced using the calculated J_{ab} values, the agreement is still far from satisfactory. In order to improve the fit, the Mo sphere radii for the K, Rb, and Me_4N salts were adjusted in proportion to their metal–metal bond distances relative to the Cs salt. This modification resulted in a very good fit with the experimental J_{ab} values as can be seen from Table 4 and Figure 11.

The success of the Xα–VB method to model and consequently predict magneto–structural correlations can be judged from a comparison of the observed versus calculated J_{ab} values reported in Table 4 and Figure 11. Clearly, once the Mo sphere are adjusted

(37) Grey, I. E.; Smith, P. W. *Aust. J. Chem.* **1969**, *22*, 121.
(38) Grey, I. E.; Smith, P. W. *Aust. J. Chem.* **1971**, *24*, 73.
(39) Daudey, J. P.; deLoth, P; Malrieu, J. P. In: *Magneto-Structural Correlations in Exchange Coupled Systems*; NATO Symposium; Gatteschi, D., Kahn, O., Willet, R. D., Eds.; Reidel: Dordrecht, The Netherlands, 1984.
(40) Noodleman, L.; Davidson, E. R. *Chem. Phys.* **1986**, *109*, 131.
(41) Nepveu, F.; Waly, L.; Haase, W.; Astheimer, H. Presented at the International Workshop on Theoretical Approaches to the description of the Electronic Structures of Transition Metal Compounds, San Miniato, Italy, April 1985.
(42) Gewirth, A. A.; Cohen, S. L.; Schugar, H. J.; Solomon, E. I. *Inorg. Chem.* **1987**, *26*, 1133.
(43) Gewirth, A. A.; Solomon, E. I. *J. Am. Chem. Soc.* **1988**, *110*, 3811.
(44) Shadle, S. E.; Penner-Hahn, J. E.; Schugar, H. J.; Hedman, B.; Hodgson, K. O.; Solomon, E. I. *J. Am. Chem. Soc.* **1993**, *115*, 767.

Table 4. Calculated Exchange Coupling Constants for $A_3Mo_2X_9$ (X = Cl, Br) Complexes Using Adjusted Mo Sphere Radii

complex	d(Mo–Mo)[14] (Å)	$-J_{ab}$ (cm^{-1}) obsd[15]	fixed[a] R_{Mo}	variable[b] R_{Mo}
$K_3Mo_2Cl_9$	2.524	560	713	539
$Rb_3Mo_2Cl_9$	2.59	491	564	488
$Cs_3Mo_2Cl_9$	2.655	414	414	414
$(Me_4N)_3Mo_2Cl_9$	2.778	275	221	304
$Cs_3Mo_2Br_9$	2.86	380	380	380
$(Me_4N)_3Mo_2Br_9$	3.12	239	67	231

[a] Calculated using R_{Mo} = 1.184 Å for chloride complexes and R_{Mo} = 1.380 Å for bromide complexes based on the best fit to J_{ab} for $Cs_3Mo_2Cl_9$ and $Cs_3Mo_2Br_9$. [b] R_{Mo} adjusted in proportion to metal–metal distance relative to the Cs salts.

on the basis of metal–metal bond distance, the Xα–VB method is able to model the observed trend in the experimental J_{ab} values remarkably well for both the chloride and bromide complexes, and this result serves to highlight its usefulness in investigating magnetic interactions in what can be regarded as strongly antiferromagnetically coupled dimers. In this particular case, however, the problem was made easier by the insensitivity of the calculated J_{ab} values to the Cl sphere radii. An obvious extension of this work which we are currently undertaking is to use the Xα–VB approach to analyze the optical spectra of $Cs_3Mo_2Cl_9$ and $Cs_3Mo_2Br_9$. This has already been done for several Cu(II) dimer complexes, but in these cases the metal–metal bonding interactions were much weaker.[9-12] In addition, the electronic spectra of the related $W_2X_9^{3-}$ (X = Cl, Br) complexes have yet to be interpreted.

Acknowledgment. Financial support of the Australian Research Council is gratefully acknowledged as well as John McGrady of The Research School of Chemistry, Australian National University, for helpful discussions in relation to the implementation of the Xα–VB method.